



**HAL**  
open science

# Fluctuating Bond Aggregation: a Numerical Simulation of Neutrally-Reacted Silica Gels

Anwar Hasmy, Éric Anglaret, Romain Thouy, Rémi Jullien

► **To cite this version:**

Anwar Hasmy, Éric Anglaret, Romain Thouy, Rémi Jullien. Fluctuating Bond Aggregation: a Numerical Simulation of Neutrally-Reacted Silica Gels. *Journal de Physique I*, 1997, 7 (3), pp.521-542. 10.1051/jp1:1997173 . jpa-00247341

**HAL Id: jpa-00247341**

**<https://hal.science/jpa-00247341>**

Submitted on 4 Feb 2008

**HAL** is a multi-disciplinary open access archive for the deposit and dissemination of scientific research documents, whether they are published or not. The documents may come from teaching and research institutions in France or abroad, or from public or private research centers.

L'archive ouverte pluridisciplinaire **HAL**, est destinée au dépôt et à la diffusion de documents scientifiques de niveau recherche, publiés ou non, émanant des établissements d'enseignement et de recherche français ou étrangers, des laboratoires publics ou privés.

# Fluctuating Bond Aggregation: a Numerical Simulation of Neutrally-Reacted Silica Gels

Anwar Hasmy<sup>(1)</sup>, Éric Anglaret<sup>(2)</sup>, Romain Thouy<sup>(2)</sup> and Rémi Jullien<sup>(2,\*)</sup>

<sup>(1)</sup> Laboratoire de Physique des Solides, Université Paris-Sud, Bâtiment 510, 91405 Orsay Cedex, France

<sup>(2)</sup> Laboratoire des Verres (\*\*), Université Montpellier II, Place Eugène Bataillon, 34095 Montpellier Cedex 5, France

(Received 29 July 1996, received in final form 7 October 1996, accepted 20 November 1996)

PACS.61.43.Bn – Structural modeling: serial-addition model, computer simulation

PACS.61.43.Hv – Fractals; macroscopic aggregates (including diffusion-limited aggregates)

PACS.82.70.Gg – Gels and sols

**Abstract.** — Numerical simulations of gel formation using the newly developed Fluctuating Bond Aggregation (FBA) algorithm are presented. This algorithm allows possible cluster deformations during aggregation by considering a tuning bond *flexibility* parameter  $F$ . Three-dimensional computer simulations show that for large  $F$ , there is a well-defined threshold value of concentration  $c$  below which the realization of all intra-aggregate bond possibilities prevents the formation of a gelling network. For  $c > c_g$ , a *true* sol-gel transition occurs at a characteristic time  $t_g$ , *i.e.* an infinite cluster (self connected through the boundary conditions) appears. In contrast to the diffusion limited cluster-cluster aggregation (DLCA) model,  $t_g$  does not increase as the box size increases. Comparison between numerical results and measurements of the gelation time of silica gels prepared in container of various sizes suggests that gelation without addition of catalyst (neutrally-reacted) and under base catalyzed conditions corresponds to large and small  $F$ , respectively. Moreover, for large  $F$  values, we calculate scattering intensity curves for FBA gels and find that they agree with experimental SANS data for neutrally-reacted silica aerogels.

## 1. Introduction

In the last decade, numerical models have been introduced to explain aggregation phenomena in polymeric and colloidal systems [1–3] and some of them appeared to be successful in modeling both experimental sol-gel process and gel structures. For example, the diffusion limited cluster-cluster aggregation (DLCA) model [4, 5] has been used to reproduce the temporal evolution of the average size [6] and size distributions of aggregates [7] as well as small angle scattering measurements during aggregation of colloidal systems [8–11]. However, some specific aspects concerning the experimental dependence of the gelation time  $t_g$  and the gel concentration  $c_g$  on the container size (where silica gels are prepared) have not yet been elucidated. The DLCA model predicts that the gelation time  $t_g$  increases [9], whereas the gel concentration  $c_g$  tends to zero [12, 13] when increasing the box size.

---

(\*) Author for correspondence (e-mail: Remi@Ldv.univ-montp2.fr)

(\*\*) UMR 5587 CNRS

The DLCA model has successfully been used to reproduce small angle neutron scattering (SANS) results on base-catalyzed silica (BCS) aerogels [13], but this model fails to reproduce the more compact structures of neutrally-reacted silica (NRS) aerogels. Aerogels are obtained from silica gels, the most currently investigated gelling systems, and can be prepared in different ways and under different chemical conditions leading to various structures [14]. When silicon alkoxydes are used, the chemical mechanisms and relative speeds of hydrolysis and condensation reactions are strongly dependent on the catalysis and the molar ratio of water [15, 16]. It is known that in the NRS case (where non condensed particles aggregate), the sol-gel process leads to tenuous structures [17]. Therefore, intra-aggregate motions should exist due to free-rotations, bond angle deformations, *etc.* This is in contrast with the BCS case, where condensed particles form in the very early stages of the growth process [15, 16, 18]. Therefore, for such catalysis conditions, the aggregation of rigid clusters is more probable, as represented in the DLCA model [4, 5].

In this paper, we modify the DLCA model and allow, in addition to rigid motions of clusters, some internal motions (cluster deformations). We use the *Bond Fluctuation* method [19, 20] which includes a bond *flexibility* parameter  $F$ , which can be tuned. Such a kinetic rule is selected primarily for a sake of efficiency and it is clear that any real dynamics would proceed differently. However, we show that this simplified representation of flexibility effects is adequate to efficiently simulate physical properties of real systems exhibiting local restructurations. With this method, we show that for large  $F$  values, the gel concentration  $c_g$  takes a well-defined value in the thermodynamic limit of large systems, and the gelation time  $t_g$  does not depend on the size of the numerical box, or system size. This last result is in agreement with experimental measurements of  $t_g$  as a function of the container size for NRS gels [21]. In contrast, we measure experimentally that for BCS gels,  $t_g$  increases with the container size as predicted by the DLCA model [9, 12]. For the structure of NRS aerogel, we calculate the scattering intensity and show that the FBA model provides a good description of the SANS experimental curves.

This article is organized as follows: in Section 2 we describe the FBA algorithm and justify the parameter values used in our simulations. For large  $F$ , we report some results about the criticality and the kinetics of the FBA model. In Section 3, we present numerical calculations of the fractal dimension  $D$  of the simulated aggregates. We also show computed scattering function curves for simulated gels at  $c > c_g$ . In Section 4, we report the preparation of silica gels and aerogels as well as the experimental methods we used. In Section 5 we compare our numerical results with experiments and we present a discussion; we finally conclude in Section 6. Short reports on the FBA model and the  $t_g$  dependence on the container size have been published elsewhere [21, 22].

## 2. Numerical Simulations of the Gel Formation

2.1. THE MODEL. — The FBA model is an extension (inclusion of aggregation) of the Bond Fluctuation algorithm which was first introduced to describe the equilibrium kinetics of linear polymers [19, 20]. The simulation is performed on a cubic lattice of unit length with sites, limited to a cubic box of edge length  $L$ . Particles are assumed to be hard cubes of edge length 2 moving by successive unit jumps on the lattice, taking care of periodic boundary conditions (PBC) at the box edges. A bond is formed permanently as soon as two particles try to overlap, afterwards the bond length is limited between 2 and  $\sqrt{10}$ , since bonding vectors between particle centers are restricted to a set of 108 possibilities:  $[\pm 2, 0, 0]$ ,  $[\pm 2, \pm 1, 0]$ ,  $[\pm 2, \pm 1, \pm 1]$ ,  $[\pm 2, \pm 2, \pm 1]$ ,  $[\pm 3, 0, 0]$ ,  $[\pm 3, \pm 1, 0]$  (and all possible permutations). The directions  $[\pm 2, \pm 2, 0]$  (and permutations) are forbidden to avoid bond crossing [20]. As in the DLCA model, the numerical simulation starts with a collection of  $N$  particles randomly positioned

in the box (avoiding overlaps). The volume fraction  $c$  is related to  $N$  by:

$$c = 8 \frac{N}{L^3}. \quad (1)$$

In addition to  $L$  and  $N$ , two extra parameters are considered as compared to DLCA, the bond flexibility  $F$  and the particle connectivity  $f$ . For  $F = 0$  the DLCA model (aggregation of rigid clusters) is recovered while for  $F \rightarrow \infty$  the motion of a cluster is due only to the random motions of its particles. The parameter  $f$  fixes the total possible number of bonds per particle. The procedure is the following: at each Monte Carlo step, a cluster of  $n$  particles is selected with a probability

$$P_n \propto \frac{1 + Fn}{1 + F} n^\alpha. \quad (2)$$

Either this cluster is moved rigidly by one unit step in a direction chosen at random among the six directions  $[\pm 1, 0, 0]$  (and permutations), or one of its particles is chosen at random and moved, with probabilities  $Q_n$  and  $1 - Q_n$ , respectively. If the chosen motion is compatible with the bond restrictions and hard core conditions, it is performed and the simulation proceeds to the next iteration. In the other case, any overlapping attempt is detected and the simulation proceeds to the next step without executing the motion. If a particle tried to overlap another particle and if they are not saturated (*i.e.* they both have less than  $f$  bonds), a new bond is created between them (if there are several bonding possibilities between particles, one is chosen at random). Therefore, in this model, a new bond is formed only when one particle tries to overlap another, as in the off-lattice DLCA model [13]. Another restriction has been added to forbid the creation of bonds triangles. The aim of this artificial (and rather technical) condition is to prevent the formation of tetrahedra which, due to the bond restrictions, could not move through large distances by successive jumps of single particles. The following expressions have been chosen for  $P_n$  and  $Q_n$ :

$$P_n = \frac{\frac{1 + Fn}{1 + F} n^\alpha}{\sum \frac{1 + Fn}{1 + F} n^\alpha}, \quad (3a)$$

$$Q_n = \frac{1}{1 + Fn}, \quad (3b)$$

where the sum runs over all the clusters and  $\alpha$  is a kinetic exponent. Knowing that, only a single particle jump is allowed per unit time, the mobility of an aggregate of  $n$  particles varies as  $1/n$  (as for linear polymers [20]), such expressions insure a cluster mobility proportional to  $n^\alpha$  for any  $F$ , as in DLCA. It is known [2, 3] that  $\alpha$  should be taken equal to  $-1/D$ , where  $D$  is the cluster fractal dimension, to insure a cluster diffusivity varying as the inverse of the radius. In all the calculations presented here we have taken  $\alpha = -0.5$ , in agreement with the resulting fractal dimension  $D$  of clusters, close to 2. As a consequence of (2), the "physical" time  $t$  is calculated by adding:

$$\delta t = \frac{1}{\sum \frac{1 + Fn}{1 + F} n^\alpha}. \quad (4)$$

at each iteration. The gelation time  $t_g$  is reached when a "true" infinite cluster appears, *i.e.* a cluster self-connected through the PBC. The simulation is stopped when a single aggregate containing  $N$  particles is formed. In a situation in which formation of saturated clusters prevents this, we stop the simulation after waiting a very long time  $t_s$ .

2.2. SELECTING A CONVENIENT SET OF PARAMETER VALUES. — More realistic Monte Carlo algorithms to simulate local restructurations during aggregation may run the risk of requiring a prohibitive amount of computational time. To our knowledge, the best way to simulate this physical phenomenon is the one we propose here. However, the advantages of the efficient bond fluctuating method are strongly dependent on the parameter values used in the simulation. For example, when the functionality  $f$  increases, the dynamics is slowed down due to bond constraints. For this reason, in almost all of our 3-dimensional simulations we have used  $f = 3$ , which is the lowest value able to produce a gel ( $f = 2$  corresponds to the interesting problem of flexible chains aggregation, which has been previously studied with a different method [23]). For the other parameters (the bond flexibility  $F$ , the final time  $t_s$  and the box size  $L$ ), we have tested different values and selected those for which the main properties of our model are recovered in a non-prohibitive computation time.

First, we examine the effect of the bond flexibility  $F$  on the number of flocs formed, *i.e.* clusters with all intra-cluster bounding possibilities saturated, since all their particles already form  $f$  bonds. For  $f = 3$  and  $L = 60$  we computed the cluster saturation probability  $p_s$  for different  $c$  values. We point out that a good estimation of the quantity  $p_s$  (which, for a single run, is equal to 1 if at least one saturated floc appears in a single run, or 0 in the opposite case) requires a large number of independent runs. The results are reported in Figures 1. In Figure 1a we considered  $t_s = 10^5 N$  and  $F = 0$  (open circles), 5 (black squares), 25 (open diamonds), 125 (black triangles) and 625 (open triangles). We observe that for  $F > 0$  and small  $c$  values,  $p_s$  is different from 0, in contrast with the DLCA case (open circles). In this limit, it can be concluded that the existence of “flocs” prevents the formation of a “gelling network”, since it prevents the formation of a single aggregate containing  $N$  particles. When  $c$  is increased,  $p_s$  vanishes, and then, in the limit of large  $c$  values, the possibility of forming a gelling network is recovered. Moreover, this figure shows that the concentration threshold value, at which  $p_s$  becomes equal to 0, increases when  $F$  increases.

Figure 1b shows plots of  $p_s$  versus  $c$  obtained from simulations carried out with  $F = 125$  and various final times:  $t_s = 2 \times 10^4 N$  (open circles),  $10^5 N$  (black triangles) and  $5 \times 10^5 N$  (open diamonds). Here, we observe that at small  $c$  values the maximum of the probability curve  $p_s(c)$  increases with  $t_s$ ; however, the concentration threshold (where  $p_s$  vanishes) is the same in all cases. A similar scenario is observed in Figure 1c, when considering  $t_s = 10^5 N$ , and the box sizes  $L = 60$  (black triangles) and  $L = 120$  (open triangles). In summary,  $L = 60$  and  $t_s = 10^5 N$  are values that allow us to study the main properties of our model: the appearance of “flocs” at small  $c$  values and the evidence for a concentration threshold above which a gelling network may form.

To select a relevant value for  $F$ , we have computed, for  $L = 60$  and  $t_s = 10^5 N$ , the normalized average cluster size  $\langle n \rangle / N$  as a function of the concentration  $c$  for different  $F$  values. The results are reported in Figure 2a for the same parameters as in Figure 1a. Here we observe that for  $c$  smaller than a gel concentration  $c_g$ , the cluster flexibility prevents gel formation since a lot of clusters appear to be saturated. For  $c > c_g$ , the gelation takes place ( $\langle n \rangle / N \rightarrow 1$ ), *i.e.* all  $N$  particles assemble to form a single cluster. Figure 2b shows how  $c_g$  depends on  $F$ . Here,  $c_g$  is defined as the  $c$ -value for which  $\langle n \rangle / N$  is equal to 0.5 (black circles), or to 0.8 (open circles). For  $F = 125$ ,  $c_g$  saturates at a value around 0.055. Hereafter, we will fix  $F = 125$ , a value for which  $c_g$  begin to behave asymptotically with increasing  $F$ , and this limit will be referred as the FBA model (or large  $F$ ), while  $F \rightarrow 0$  will be referred as the DLCA model (or small  $F$ ).

2.3. THE CONCENTRATION THRESHOLD. — The above results show the existence of a critical concentration  $c_g$ . One interesting point is to test whether  $c_g$  is still defined in the thermodynamic limit of large systems. This has been investigated by observing how  $c_g$  behaves when

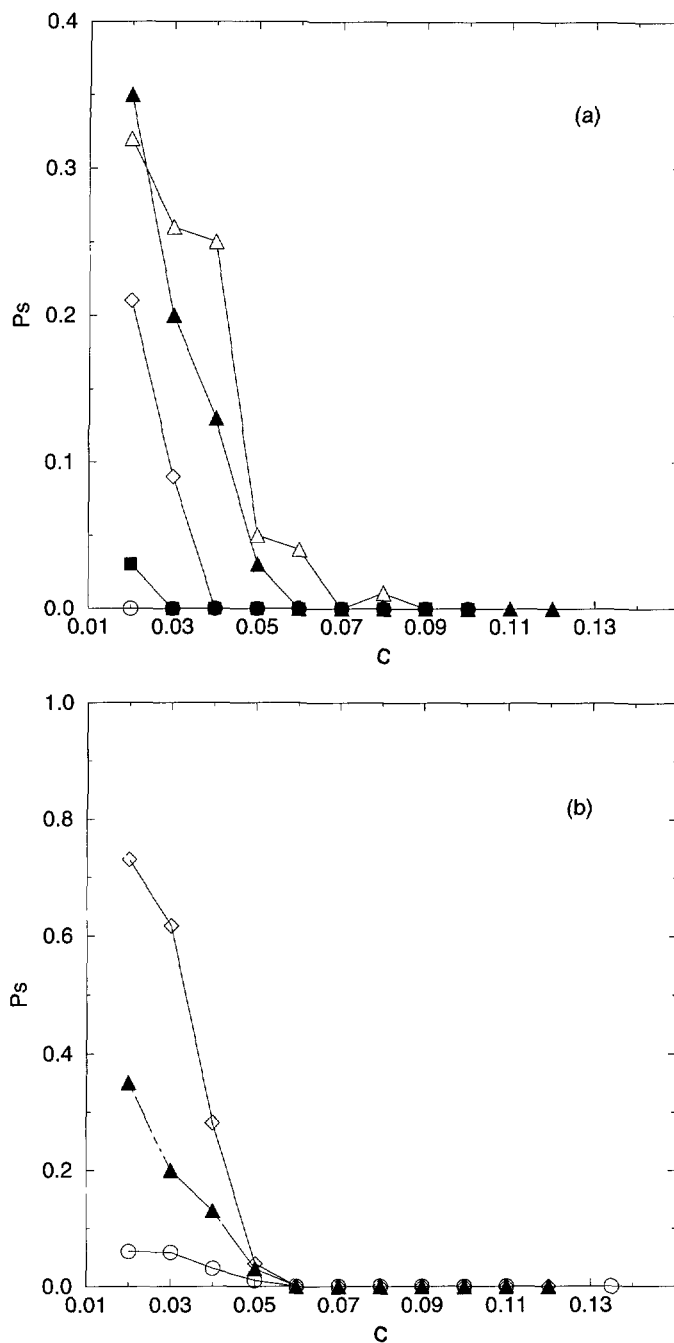


Fig. 1. — Plot of the average cluster saturation probability  $p_s$  as a function of the concentration  $c$ , for  $f=3$ , (a)  $L=60$ ,  $t_s=10^5 N$  and  $F=0$  (open circles), 5 (black squares), 25 (open diamonds), 125 (black triangles) and 625 (open triangles). (b)  $L=60$ ,  $F=125$  and  $t_s=2 \times 10^4 N$  (open circles),  $10^5 N$  (black triangles) and  $5 \times 10^5 N$  (open diamonds). (c)  $F=125$ ,  $t_s=10^5 N$  and  $L=60$  (black triangles) and  $L=120$  (open triangles). These data result from an average over 50 and 10 independent simulations for  $L=60$  and 120, respectively.

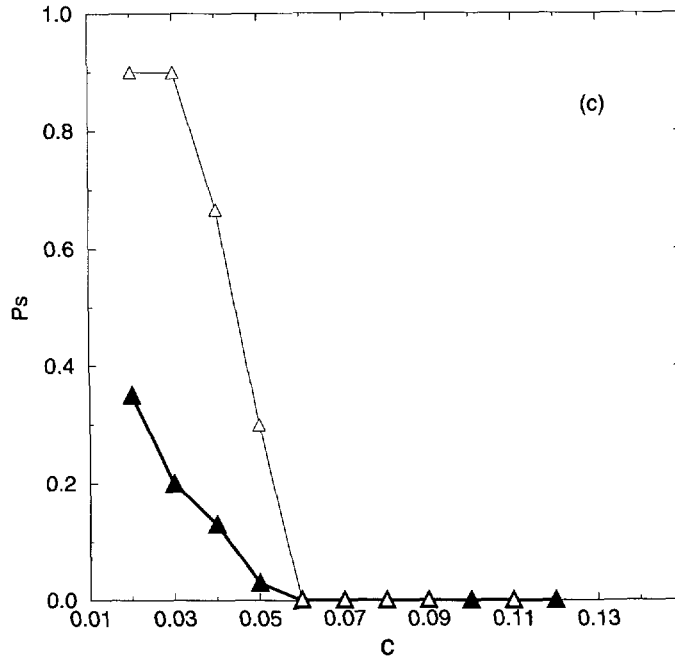


Fig. 1. — (Continued).

the box size  $L$  is increased. These results are presented in Figures 3 (for similar parameters as Fig. 1c). Data corresponding to  $\langle n \rangle / N$  as a function of  $c$  is reported in Figure 3a. The transition is more abrupt for the largest box size and  $c_g$  is independent on  $L$ . In fact, when  $L$  is increased, the average size  $\langle n \rangle / N$  exhibits similar behavior as the probability  $P_\infty$  that a given particle belongs to an “infinite” cluster in percolation theory [24]. On the other hand, in our simulations we observed that for  $c \geq c_g$ , one single cluster becomes self-connected *via* the PBC at a given time  $t_g$ , *i.e.* a true *infinite* cluster appears. Such a criterion defines a gel better than the one previously used in the DLCA [12, 13] model. We calculated the gelation probability  $p_g$ , *i.e.* the probability that, at a given concentration, a cluster becomes self-connected *via* PBC. The results of  $p_g$  *versus*  $c$  are reported in Figure 3b. Once again, we observe a transition between two regimes, which is more abrupt for the largest box size. We recall that such a behavior is typical for systems supporting a phase transition [25].

Another interesting quantity to study is the mean radius of gyration  $R_g$  given by:

$$R_g^2 = \frac{1}{N} \sum_{i=1}^{N_j} (\mathbf{r}_i - \mathbf{r}_j)^2 \quad (5)$$

where  $\mathbf{r}_i$  measures the position of a particle  $i$  belonging to an aggregate  $j$  and  $\mathbf{r}_j$  is the center of mass of this aggregate. To insure a better calculation than the one usually performed for  $R_g$ , we extracted out of the box the cluster, taking the PBC into account. In Figure 3c we show our numerical results for  $R_g$  as a function of  $c$ . As expected, the divergence observed at  $c_g$  is more pronounced for the largest box size  $L (= 120)$ . For  $c \geq c_g$ ,  $R_g$  corresponds to the radius of gyration of the single cluster obtained at the end of the aggregation process. Hence, it is interesting that, in this limit,  $R_g$  decreases when  $c$  increases (see Fig. 3c). We recall

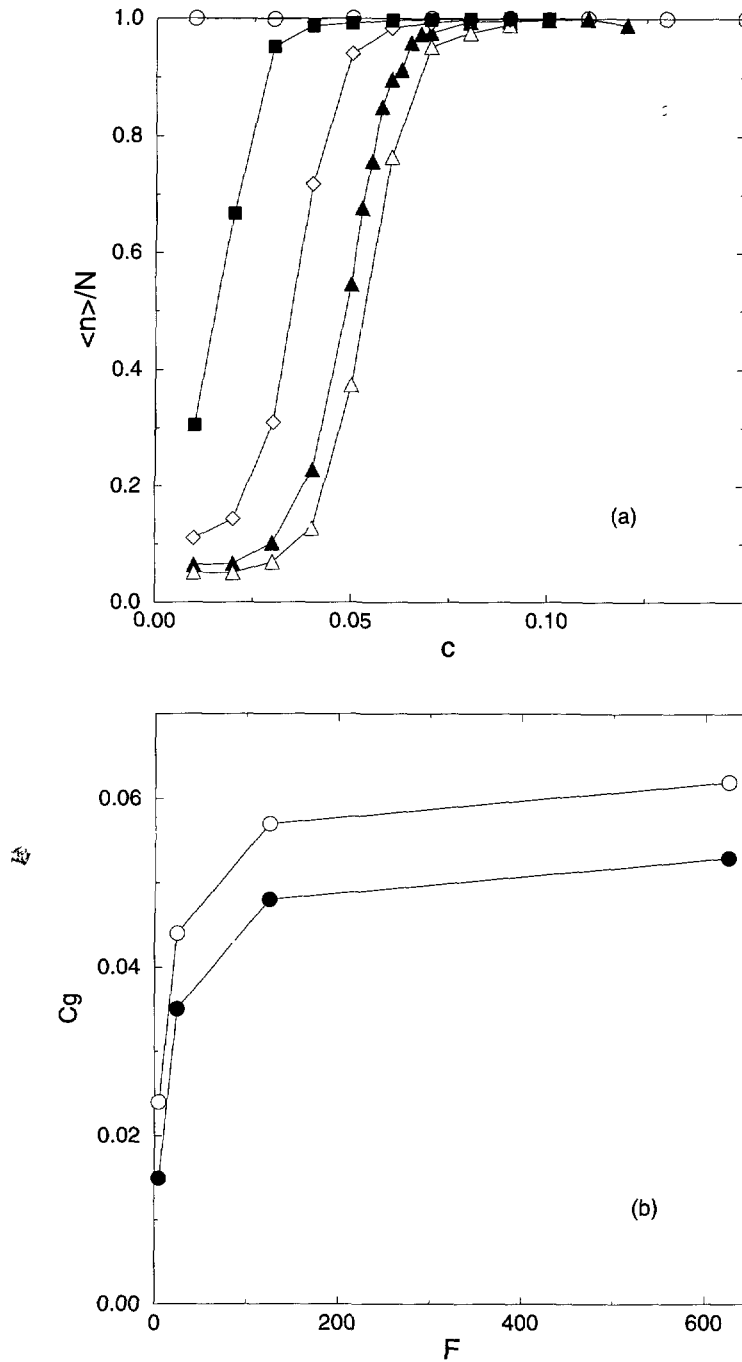


Fig. 2. — a) Plot of the normalized average cluster size  $\langle n \rangle / N$  as a function of  $c$ , for same parameters and number of runs as in Figure 1a. b)  $c_g$  as a function of  $F$  ( $c_g$  is defined as the  $c$ -value for which, in Fig. 2a,  $\langle n \rangle / N$  is equal to 0.5 (black circles), and equal to 0.8 (open circles)).

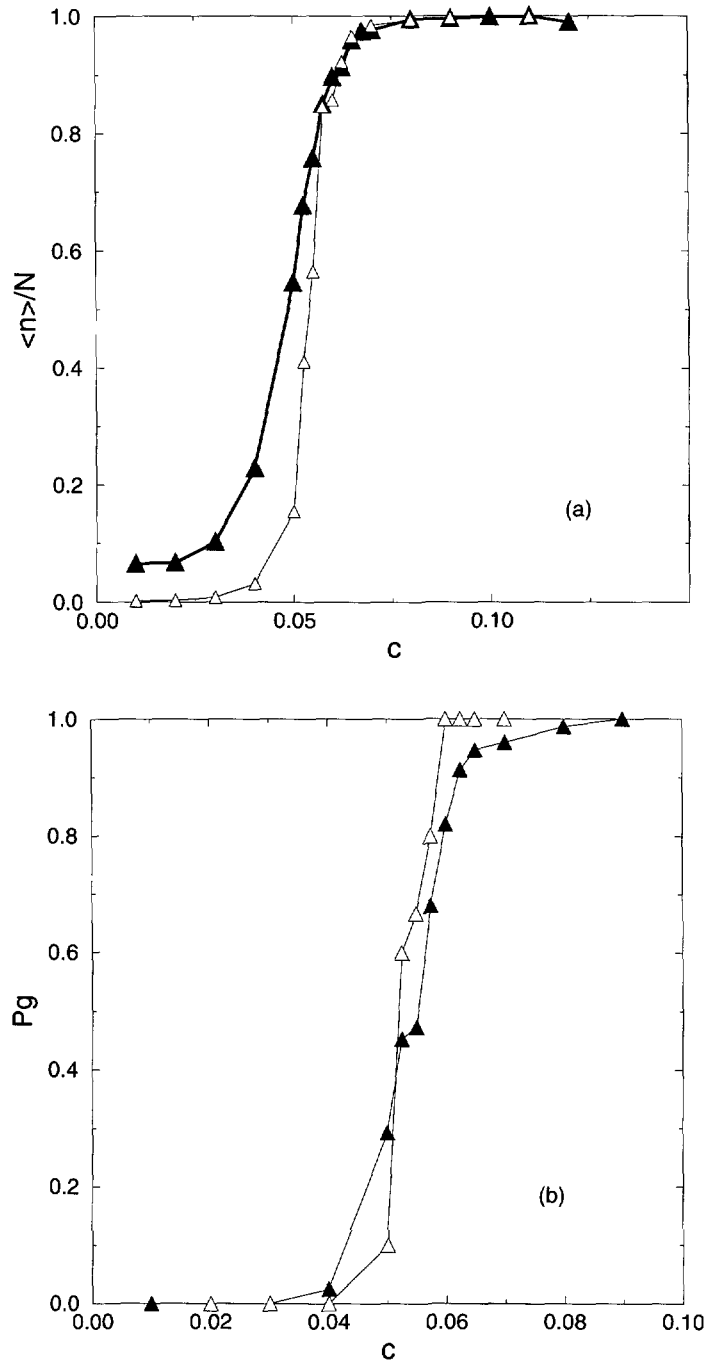


Fig. 3. — For  $f = 3$ ,  $t_s = 10^5 N$ ,  $F = 125$  and two different box sizes  $L = 60$  (black triangles) and  $L = 120$  (open triangles) we show: a)  $\langle n \rangle / N$  versus  $c$ , b)  $p_g$  versus  $c$ , and c)  $R_g$  versus  $c$ . These data result from an average over 50 and 10 independent simulations for  $L = 60$  and 120, respectively.

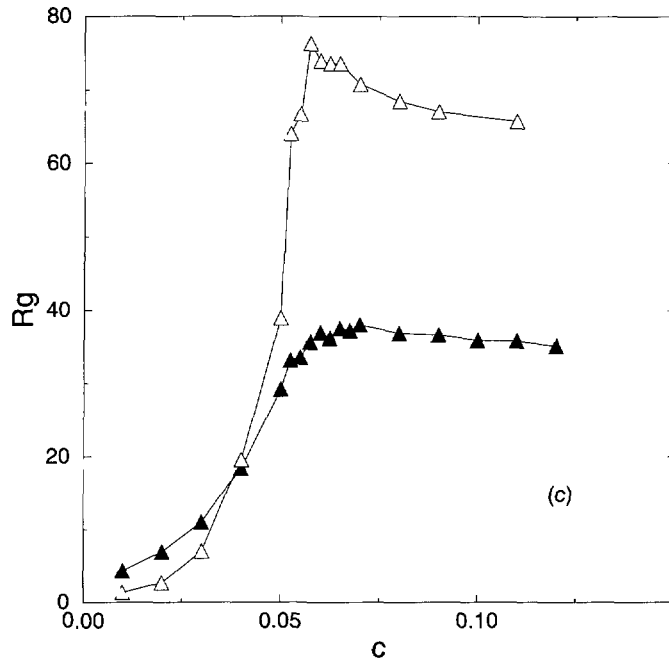


Fig. 3. — (Continued).

that the correlation length  $\xi$  (corresponding to the crossover from fractal behaviour on short length scales to a uniform structure on long length scales) also decreases when  $c$  increases and vanishes at a very high concentration [13, 26]. In fact, when calculating  $R_g$  with the gelling system extracted out of the box, the contribution of cluster branches leads to  $R_g > L/2$ ; however, since  $\xi$  vanishes at a very high  $c$  value, it is expected that at high concentration,  $R_g$  reaches the expected value  $L/2$  for a gelling network.

The existence of a phase transition is demonstrated by the non-dependence of  $c_g$  on  $L$ , since this indicates that the critical concentration  $c_g$  is well defined in the thermodynamic limit of large systems. This is not the case with DLCA since, as mentioned above,  $c_g$  tends to 0 when  $L$  increases. From our FBA data, we estimate the critical gelling concentration  $c_g$  to be approximately equal to 0.055. Unfortunately, a larger precision in the measure of  $c_g$  (which could be useful in an eventually analysis and determination of critical exponents) is hard to be obtained at the present time, because of the very large computer resources that would be required.

**2.4. TEMPORAL EVOLUTION OF THE RADIUS OF GYRATION.** — As mentioned above, a self-connected cluster appears at a time  $t_g$ . To demonstrate clearly the existence of  $t_g$ , we computed the radius of gyration  $R_g$  at each iteration time. In Figure 4a we show a log-log plot of  $R_g$  versus  $t$  for the selected set of parameters ( $L = 60$ ,  $F = 125$ ,  $f = 3$ ,  $t_s = 10^5 N$ ) and different concentrations values,  $c = 0.03, 0.05, 0.1, 0.15$  and  $0.2$ . The arrows indicate the computed gelation time  $t_g$  at which a self-connected cluster appears. For  $c \leq 0.05$ ,  $t_g$  is not reached since no self-connected cluster appears after waiting until the final time  $t_s = 10^5 N$ . Note that for  $c > 0.05$ ,  $t_g$  coincides with the first maxima of  $R_g(t)$  curves. As expected, these maxima approximately correspond to  $R_g = L/2$ , and shift towards the small  $t$  values when  $c$  increases.

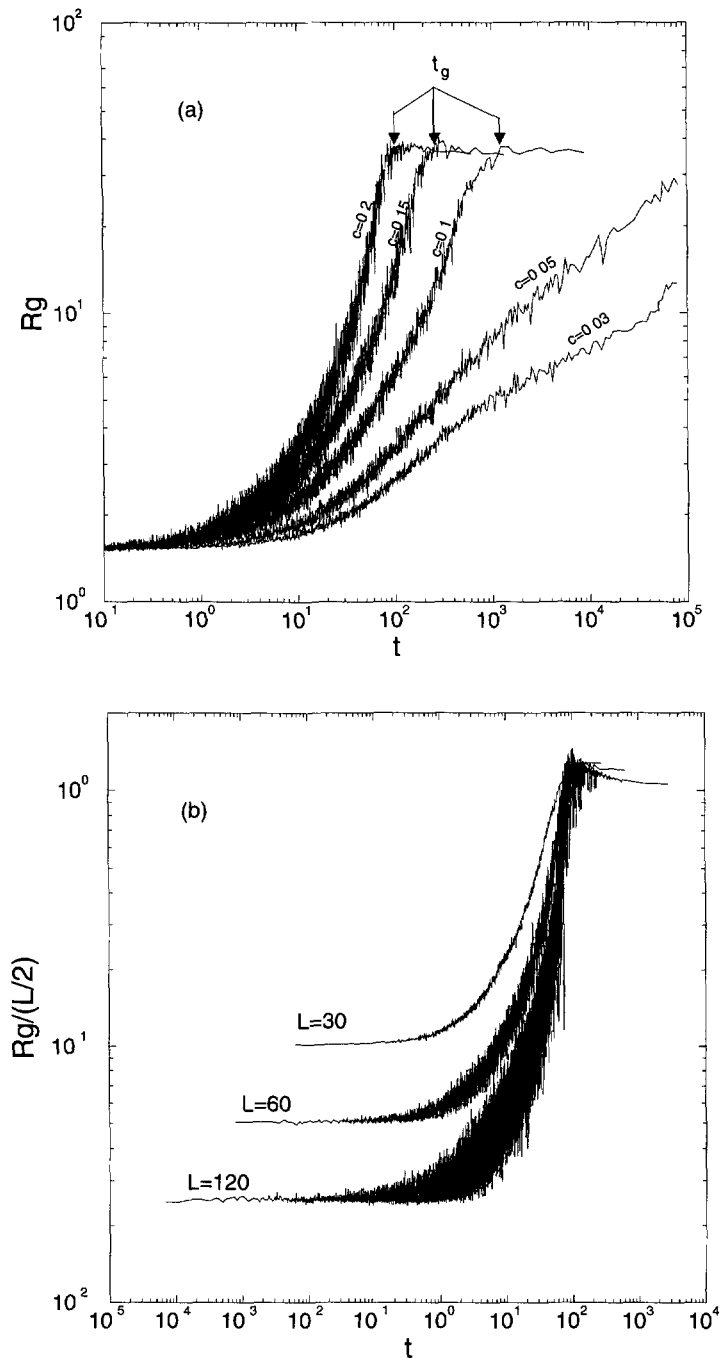


Fig. 4. — Log-log plot of the temporal evolution of: a)  $R_g(t)$  for different concentration values and  $L = 60$ ; and b)  $R_g(t)/(L/2)$  for  $c = 0.2$  and different box sizes. These data result from an average over 200, 50 and 10 independent simulations for  $L = 30, 60$  and  $120$ , respectively.

Moreover, for  $c > c_g$ , we conclude from these curves that our results are independent of the arbitrary choice of the parameter  $t_s$  ( $= 10^5 N$ ), since a single aggregate is obtained at a time much smaller than  $t_s$ .

In Figure 4b we show the temporal evolution of the normalized radius of gyration  $R_g/(L/2)$  for  $c = 0.2$ , the same parameters as in Figure 4a, and various  $L$  values:  $L = 30$ ,  $L = 60$  and  $L = 120$ . We observe that the maximum is located for each curve at the same  $t$ . This suggests that in contrast to the DLCA model,  $t_g$  is independent on the box size in the FBA model. In other words,  $t_g$  seems to be well-defined in the thermodynamic limit of large systems (as  $c_g$  does). This last result, will be discussed in Section 5 when comparing with experiments. But, in a recent publication [27], it has been shown that the non dependence on  $L$  of  $t_g$  also results when considering a DLCA model without PBC and with a sticking rule between clusters different than those considered for this model. Another interesting point is illustrated by the above figure: for  $t > t_g$ ,  $R_g$  decreases slowly due to a relaxation mechanism. This result is quite original (when comparing to aggregation models of rigid clusters), since it directly relates to the restructuring mechanism allowed in the FBA model.

**2.5. DYNAMICAL SCALING OF THE CLUSTER SIZE DISTRIBUTION.** — It is interesting to examine the clusters size distribution, since it provides information about the evolution of the system. We computed the number of clusters  $N_n(t)$  (excluding the largest cluster) as a function of the size  $n$  at different times smaller than  $t_g$ . Figure 5a shows the function  $N_n(t)$  for  $c = 0.07$  and the selected set of parameters ( $L = 60$ ,  $f = 3$ ,  $F = 125$ ). In all cases the curves exhibit a maximum at very small cluster sizes. Again, the FBA results are in contrast to the DLCA results, since it has been recently shown that this maximum only shows up at low concentrations ( $c < c_g$ ) [28]. According to dynamical scaling assumptions [29], it is expected that the function  $N_n(t)$  scales as [30]:

$$N_n(t) = N_o \langle n(t) \rangle^{-2} f\left(\frac{n(t)}{\langle n(t) \rangle}\right) \quad (6)$$

where  $\langle n(t) \rangle$  is the average size of clusters at a time  $t$ ,  $N_o$  is the total number of particles in the box excluding the number contained in the largest cluster, and  $f(n(t)/\langle n(t) \rangle)$  is a scaling function. We computed  $N_n(t)$  for seven different times (smaller than  $t_g$ ) and two different concentrations ( $c = 0.07$  and  $c = 0.1$ ) and find that the curves do not collapse onto a single master curve in the manner described by equation (6). However, when  $\langle n(t) \rangle$  is replaced by the weighted average:

$$\langle n_w(t) \rangle = \frac{\sum n(t)^2 N_n(t)}{N_o} \quad (7)$$

in equation (6), a good data collapse is obtained (see Fig. 5b). Figure 5c shows results for the DLCA case ( $F = 0$ ) with the same parameters as for Figure 5b. The fact that the curves collapse only when considering the weighted average size  $\langle n_w(t) \rangle$  is consistent with results reported by Lach-hab *et al.* for the DLCA case [28]. Using relation (6), these authors found out that the  $N_n(t)$  curves only collapse at low concentrations. Also, we would like to recall that this relation has been successfully used only in colloidal aggregation experiments at low concentrations [30]. When comparing Figures 5b and 5c, it can be seen that the polydispersity slightly decreases in the FBA model (compared to DLCA). This is a consequence of the kinetical contributions related to the bonds flexibility. In fact, as demonstrated in reference [31], the function  $N_n(t)$  strongly depends on the choice of the kinetical rules.

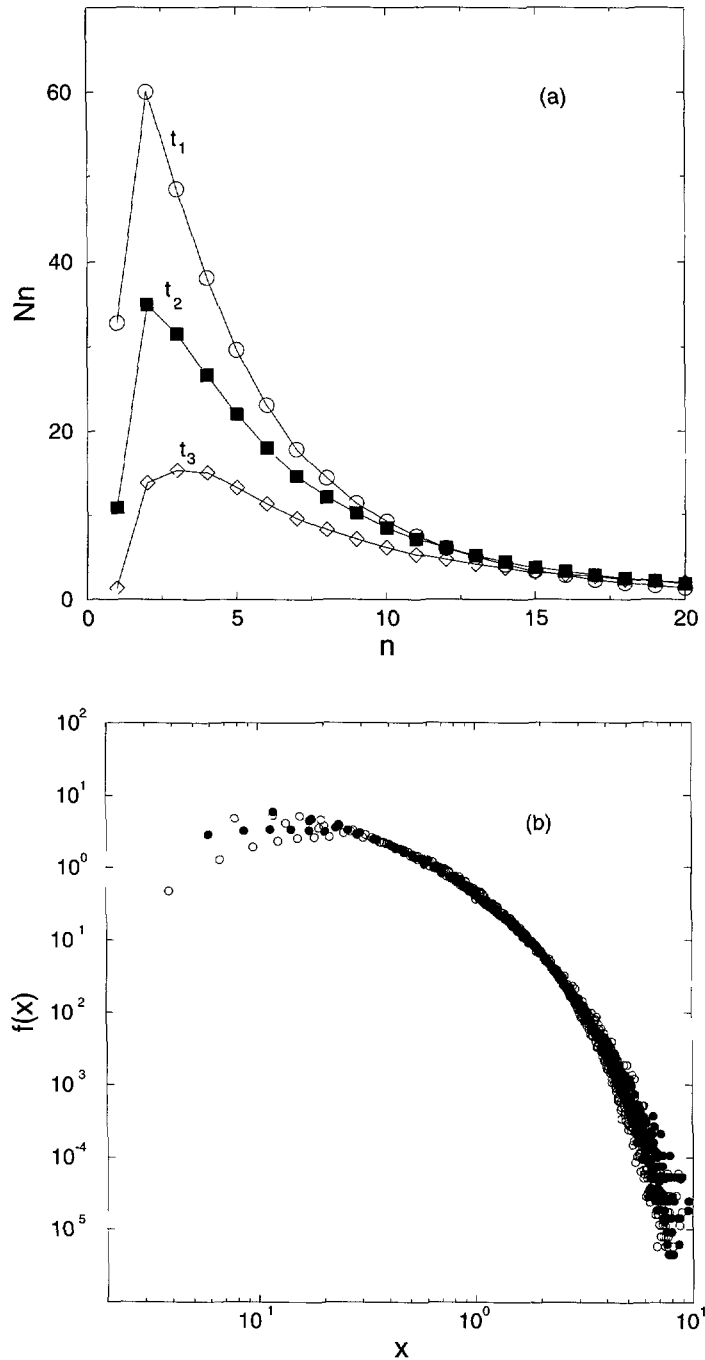


Fig. 5. — For  $f = 3$  and  $L = 60$ , we plot (a)  $N_n(t)$  as a function of the size  $n(t)$  for  $c = 0.07$ ,  $F = 125$ , and different times  $t_1 < t_2 < t_3 < t_g$ . For  $c = 0.07$  (open circles) and  $c = 0.1$  (black circles) we plot, for data obtained at various times ( $t < t_g$ ), the single master curve  $f(x)$  ( $x = n(t)/\langle n_w(t) \rangle$ ) in the FBA case (b) and in the DLCA case (c). These data result from an average over 400 simulations.

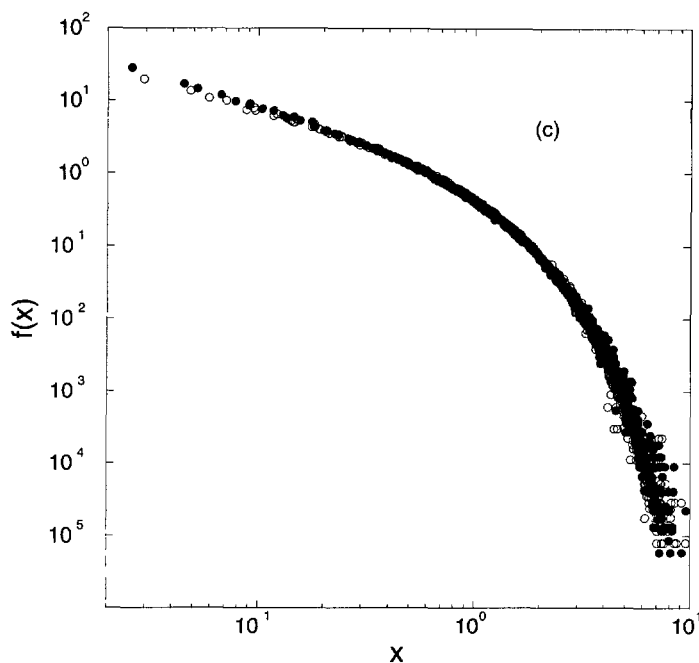


Fig. 5. — (Continued).

### 3. Some Physical Properties of the Numerical Gels

3.1. THE FRACTAL DIMENSION. — The gels obtained by cluster-cluster aggregation processes exhibit a fractal structure. For DLCA aggregates it is known that the fractal dimension  $D$  is equal to 1.8. For  $c > c_g$ , two structure domains can be distinguished, limited by the so-called fractal persistence length  $\xi$ . For distances  $r$  smaller than  $\xi$  the mass  $m$  of the system scales as  $r^D$ , and for  $r$  larger than  $\xi$ ,  $m$  scales as  $r^3$ . In other words, for  $c > c_g$ , the simulated gels exhibit fractal and an homogeneous structures at small and large distances, respectively [13]. The length  $\xi$  relates to the average size of the fractal clusters forming the numerical gel. It has been shown that in the fractal regime, the exponent  $D$  slightly increases with  $c$  [9, 28, 32], while the characteristic length  $\xi$  decreases [13].

We investigated the scaling of  $m$  with  $r$  (the number of particles  $m$  contained in a sphere of radius  $r$ ), and found, for  $c < c_g$  ( $= 0.005$ ),  $D = 2$  for FBA aggregates, a value larger than the measured ( $D = 1.8$ ) for DLCA aggregates at the same concentration (see Fig. 6a). In the FBA model, as a consequence of bond flexibility (which leads to bonds saturations), a cluster has to explore several sticking possibilities to find available bonds on another cluster. Therefore the efficiency of collisions is very weak as in the chemically-limited (also called reaction-limited) cluster-cluster aggregation CLCA (RLCA) mechanism [33, 34] (in contrast to DLCA, this model simulates aggregation with a very small sticking probability between clusters). This explains why in FBA (and also in RLCA) the aggregates are more compact than in DLCA ( $D_{\text{FBA}} > D_{\text{DLCA}}$ ).

In the gelation regime ( $c > c_g$ ), we computed  $m(r)$  for different  $c$  values, and examined how  $D$  depends on  $c$ . In contrast to the DLCA results, we were unable to obtain evidence for any slight increase of  $D$  with  $c$ . It may be because we have only worked with concentrations up to

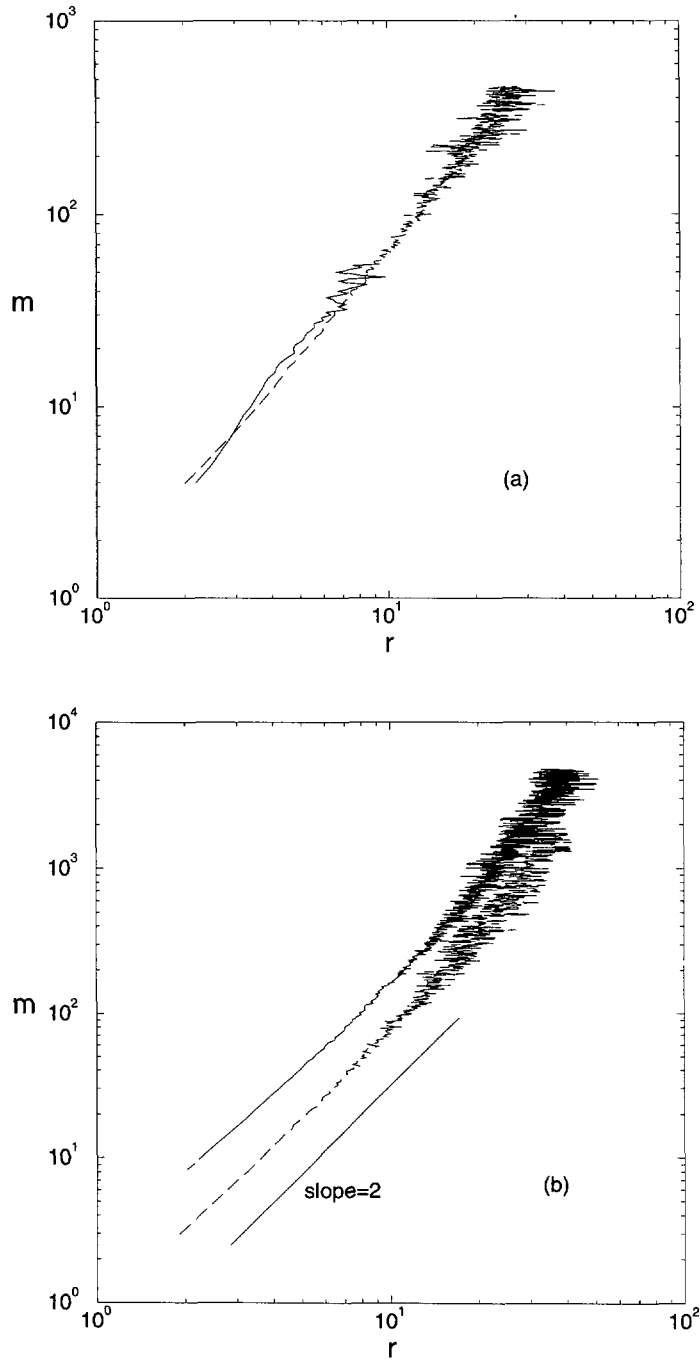


Fig. 6. — Log-log plot of  $m$  versus  $r$  for: a)  $c = 0.005$ ,  $L = 90$ , and b)  $c = 0.065$ ,  $L = 60$ ; and for  $F = 0$  (dashed line) and  $F = 125$  (solid line). The curves have been arbitrarily vertically shifted for convenience. These data results from an average over 50 simulations.

$c = 0.2$ , a value not so far from the concentration threshold  $c_g \approx 0.055$ . The effect could also be reduced here, since  $m(r)$  has been calculated after extracting the aggregate out of the box (therefore, the effective concentration becomes smaller than the initial  $c$ ). Figure 6b compares the DLCA and FBA  $m(r)$  curves, for  $c = 0.065$ . In both cases a crossover occurs; its position is related to  $\xi$ . For  $r < \xi$ , we see that while  $D$  increases in the DLCA case (when comparing with Fig. 6a, from 1.8 to 2), it remains almost constant ( $D = 2$ ) in the FBA case. It should be pointed out that the mass-distance analysis is inadequate when investigating the scaling region corresponding to very small distances [35]. From images of some FBA aggregates [36], we have evidenced that in the FBA case the system becomes compact at very small scales, surely as a consequence of the bond flexibility which allows a local restructuring mechanism.

**3.2. THE SCATTERING FUNCTION.** — The scattering function  $S(q)$  (also called the structure factor) is a useful tool for describing the structure since it mirrors the different correlation domains of the gel [17, 37, 38]. Here,  $q$  is the scattering wavevector given by

$$q = \frac{4\pi}{\lambda} \sin \frac{\theta}{2} \quad (8)$$

where  $\theta$  is the scattering angle and  $\lambda$  the wavelength of the incident beam. Analysis of  $S(q)$  leads to the determination of two characteristic lengths, namely the average size  $a$  of the particles and the fractal persistence length  $\xi$ . Three domains, corresponding to different range of wavevectors  $q$ , can generally be distinguished. At large  $q$  ( $q > a^{-1}$ ),  $S(q)$  exhibits damped oscillations, characteristic of short range correlations, as extensively discussed elsewhere [39]. At intermediate values of  $q$  ( $\xi^{-1} < q < a^{-1}$ ), the fractal nature of intra-cluster particle correlations induces a power law behavior  $S(\mathbf{q}) \sim q^{-D'}$ , where  $D'$  is an apparent fractal dimension of the clusters. Finally, at small  $q$  values, for  $q < \xi^{-1}$ ,  $S(q)$  saturates and eventually decreases as  $q$  tends to zero.

From single scattering theory, it can be shown that  $S(\mathbf{q})$  is proportional to the square of the Fourier transform of the density distribution in direct space [40, 41]; it can be therefore calculated by

$$S(q) = \langle |\sum_{\mathbf{r}} (\rho(\mathbf{r}) - \bar{\rho}) e^{i\mathbf{q}\cdot\mathbf{r}}|^2 \rangle \quad (9a)$$

or,

$$S(q) = \sum_{\mathbf{r}_1} \sum_{\mathbf{r}_2} (\rho(\mathbf{r}_1)\rho(\mathbf{r}_2) - \bar{\rho}^2) \frac{\sin q|\mathbf{r}_1 - \mathbf{r}_2|}{q|\mathbf{r}_1 - \mathbf{r}_2|} \quad (9b)$$

where  $V = L^3$ ,  $\bar{\rho} = N/V$ ,  $\langle \dots \rangle$  indicates an average over the  $\mathbf{q}$  directions,  $\rho(\mathbf{r}) = 1$  if the site  $\mathbf{r}$  is occupied by a particle center and  $\rho(\mathbf{r}) = 0$  otherwise. As discussed in [13], it is essential, when dealing with a gel, to subtract  $\bar{\rho}$  to avoid finite size artifacts due to the box.

In Figure 7 we present numerical  $S(q)$  curves calculated for  $L = 60$ ,  $f = 3$ ,  $F = 125$  and  $c > c_g$ ,  $c = 0.055, 0.065$  and  $0.075$  (solid curves), and for  $F = 0$  and  $c = 0.065$  (dashed curve). We recall that  $q$  is here a dimensionless quantity which is, in fact, equal to  $Qa$  where  $Q$  is the dimensioned wavevector and  $a$  is the size of the primary particles and, also that,  $S(q)$  has been normalized to unity for large  $q$ . The log-log curves exhibit a qualitative shape similar to that discussed in a previous work [13] for DLCA, *i.e.* a maximum at low- $q$ , which shifts to larger  $q$  as the concentration increases, an intermediate linear regime, and damped oscillations at high  $q$ -values. However, the FBA curves exhibit quantitative differences than DLCA (dashed curve) and it turns out that the absolute value of the slope in the fractal range ( $\simeq 2.3$ ) is

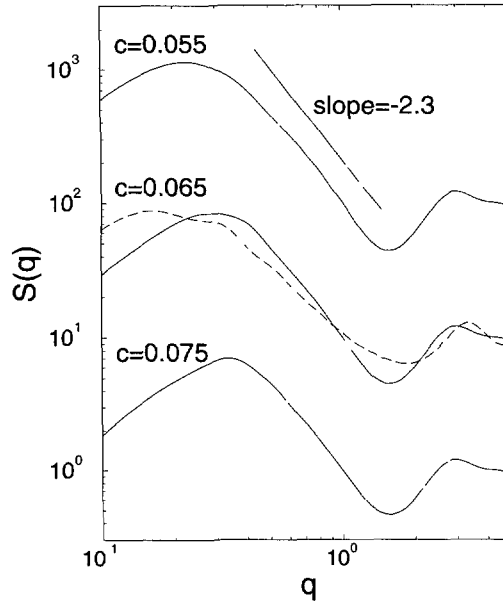


Fig. 7. —  $S(q)$  curves calculated for  $f = 3$ ,  $L = 60$ ,  $F = 125$  and three values of concentrations. For comparison the curve corresponding to  $c = 0.065$ ,  $F = 0$  is shown (dashed line). The curves have been arbitrarily vertically shifted for convenience. These data results from an average over 50 simulations.

significantly larger than that for DLCA. These results are surprising, since we reported that the fractal dimension of the aggregates forming the gel is quite similar in both cases (see Fig. 6b). Actually, the slopes  $D'$  in  $S(q)$  are, in both cases, quite different from  $D$  (it is larger in the FBA case, and smaller in the DLCA case).

Finally, we calculated a  $S(q)$  curve for  $L = 120$  and  $c = 0.065$  (the other parameters are the same as before) in order to test the effect of the box size, but this result is not presented since the curve would superimpose the  $L = 60$  curve of Figure 7. Furthermore, we would like to point out that as a consequence of neglecting density fluctuations in our calculations of the scattering function, our  $S(q)$  “artificially” tends to 0 when  $q$  tends to 0. For this reason, the behavior of  $S(q)$  at very small  $q$  values has been omitted in Figure 7.

#### 4. Experimental Methods

4.1. THE GELS. — In this section, we describe the method that we used to test the experimental  $t_g$  dependence on the container size. The gels were prepared by hydrolysis of tetramethoxysilane (TMOS) in ethyl alcohol without adding any catalyst in the NRS case, and with a 0.05N ammonia-water solution for BCS. We used four moles of water solution per mole of TMOS and various amounts of alcohol. Under acid (or neutral) catalysis, hydrolysis takes place preferably on monomers or weakly condensed species which condense preferentially with clusters [15]. The resulting gel is “polymeric-like” and has a weakly branched structure. Inversely, under basic catalysis, hydrolysis occurs on non condensed species or hydrolyzed monomers [15] so that dense particles are allowed to growth before they condensate to form the gel. This leads to a so-called “particulate” or “colloidal” structure. Each gel was prepared simultaneously in three glassy cylindrical containers of diameters 10 mm, 14 mm and 32 mm.

In order to test the effect of the container surface, some gels were also prepared in plastic containers. All containers were then hermetically closed and the gels allowed to form either at room temperature (BCS case) or at 40 °C (NRS case) in order to reduce the reaction times. The criterion to determine  $t_g$  was the non-flow of the gel when the container was tilted. It might be argued that such an experimental procedure to estimate  $t_g$ , even if it is done with the maximum of care, is quite rough and could produce systematical errors (because tilting the container may break the gel). However, we have used systematically the same procedure for all TMOS concentration, and we have verified that the results were reproducible. This method allows  $t_g$  to be estimated with a relative error of  $\Delta t_g/t_g < 10\%$  which includes both the difference between two successive measurements and the error on the visual determination of the non-flow threshold. The quantity of solution put in each container was large enough so that the volume/surface ratio was rather independent of the height  $h$  of solution. Under these conditions, we checked that  $t_g$  was independent of  $h$  in a given container.

**4.2. THE AEROGEL STRUCTURES.** — To obtain silica aerogels, the gels are dried above the critical conditions of the solvent (see [14] and references therein) so that the main structural features of the gel are preserved in the aerogel. According to the catalysis conditions used for the gel synthesis, we distinguish between BCS and NRS aerogels, respectively, which present basically different structures [45]: BCS aerogels [42] are formed with pretty well-defined poly-disperse colloidal silica particles while for NRS aerogels [17], particles are ill-defined and their average size extends down to the atomic scale. Therefore, NRS aerogels are more tenuous than BCS aerogels.

As revealed by the scattering intensity  $I(q)$  measured by Small Angle X-rays Scattering (SAXS) or Small Angle Neutron Scattering (SANS) experiments [13, 17, 42, 43], an aerogel is made of a disordered (but homogeneous in average) array of connected fractal clusters (with a size that is approximately equal to  $\xi$ ). For aerogels, the scattering intensity curves (and the scattering function  $S(q)$ ) exhibit a maximum at  $q \approx \xi^{-1}$  at low- $q$  values, and a fractal regime for  $a^{-1} < q < \xi^{-1}$ . At high  $q$ -values, in contrast to  $S(q)$ ,  $I(q)$  mirrors density fluctuations associated with the particle surface, so that for smooth particles,  $I(q)$  follows the Porod law  $I(q) \sim q^{-4}$  [44].

## 5. Comparison Between Simulations and Experiments

**5.1. THE GELATION TIME.** — We first report on the experimental measurements of  $t_g$  for BCS and NRS gels. In Figure 8,  $t_g$  is plotted as a function of the TMOS volume fraction  $\phi$  for different container diameters 10 mm (circles), 14 mm (squares) and 32 mm (diamonds). We observe that in the NRS case (Fig. 8a), the curves are almost superimposed whereas for BCS (Fig. 8b), the differences are clearly larger than the error bars indicating that  $t_g$  increases with the container diameter.

The numerical results for  $t_g$ , averaged over a large number of independent runs are reported as a function of the particle volume fraction  $c$  in Figures 9. We used the FBA model with  $f = 4$  (in agreement with the silicon functionality) and  $F = 125$  (Fig. 9a) or  $F = 0.5$  (Fig. 9b), and three different box sizes  $L = 30$  (circles), 60 (squares) and 120 (diamonds). The main result is that while  $t_g$  is almost  $L$ -independent for the large  $F$  value, it increases with  $L$  for the small  $F$  value.

When comparing Figures 8 and 9, the qualitative agreement between experiments and simulations turns out to be extremely good if the NRS and BCS cases correspond to large and small flexibility, respectively. The gelation time decreases with concentration in both BCS and NRS and this is recovered in the simulation. Even if the numerical gelation times cannot be

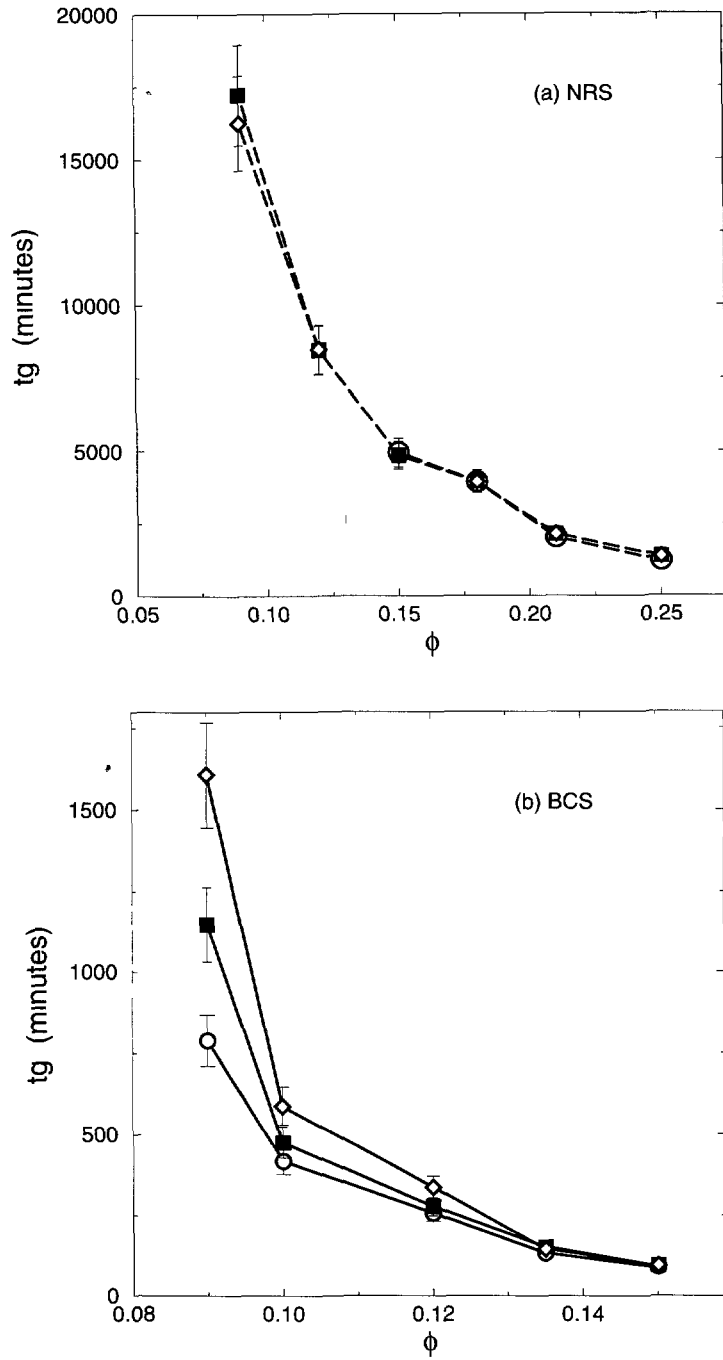


Fig. 8. — Experimental dependence of the gelation time  $t_g$  with the TMOS volume fraction  $\phi$  for various container diameters: 10 mm (circles), 14 mm (squares) and 32 mm (diamonds). Cases (a) and (b) correspond to NRS and BCS gels, respectively.

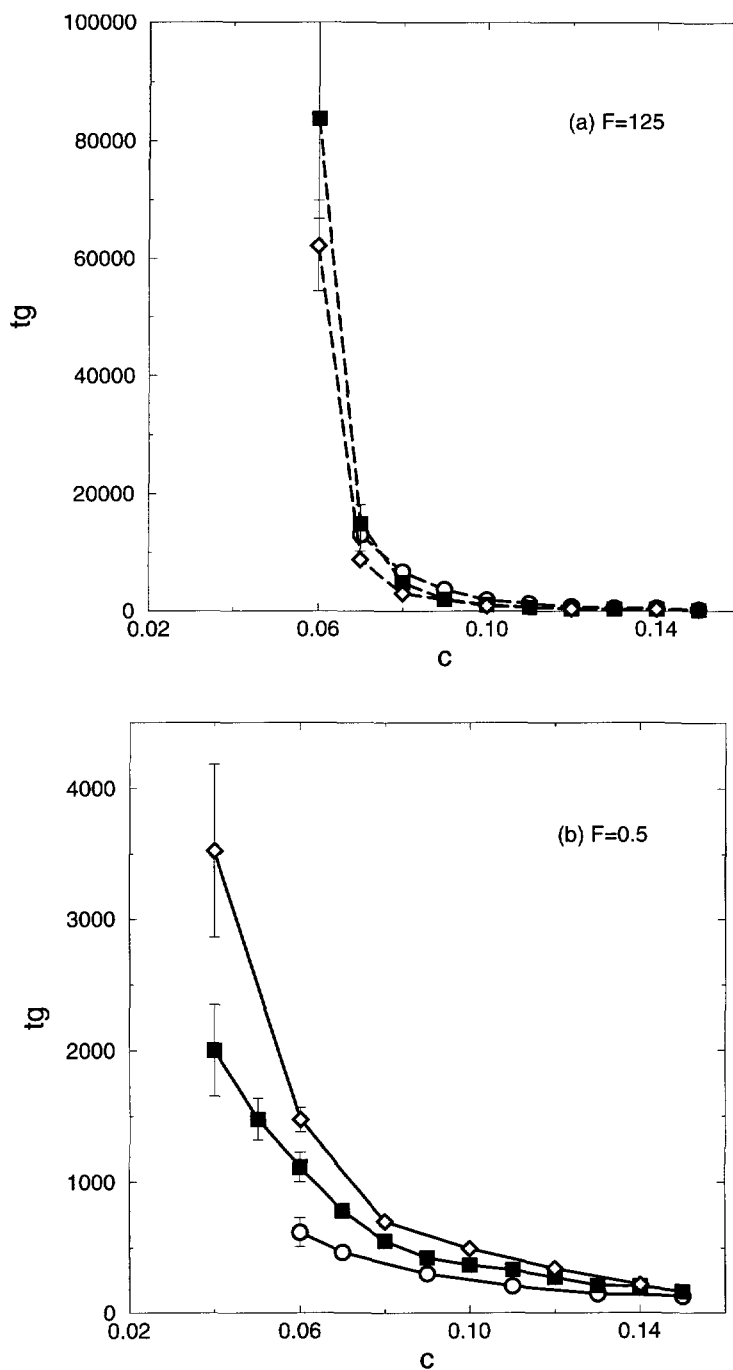


Fig. 9. — Numerical dependence of the gelation time  $t_g$  on the volume fraction of particles  $c$  calculated with the FBA model with  $f = 4$  and different box sizes  $L$ . Circles, squares and diamonds correspond to  $L = 30, 60, 120$  and cases (a) and (b) correspond to  $F = 125$  and  $0.5$ , respectively. In case (a),  $t_g$  results from an average over 400, 80 and 20 runs and in case (b), over 400, 250 and 80 runs for  $L = 30, 60$  and  $120$ , respectively.

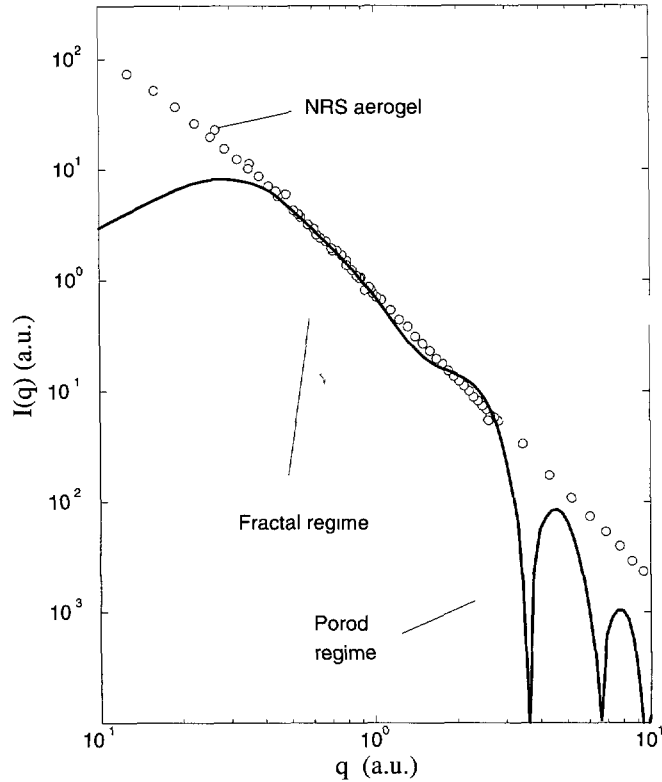


Fig. 10.— Comparison between a numerical  $I(q)$  curve for a FBA gel (solid line) and an  $I(q)$  experimental curve for a NRS aerogel (circles).

compared quantitatively to the experimental ones, their relative values are larger in the NRS case compared to the BCS case in both the simulations and the experiments. Moreover, in both simulations and experiments,  $t_g$  is almost constant in the NRS case while it increases with the box (container) size in the BCS case. Also, our finding that NRS and BCS correspond to large and small flexibility, respectively, is in agreement with what is known on the structure of the samples [45] since, as already mentioned, the BCS aerogels are made of strongly bonded mesoscopic silica particles and are therefore certainly much more rigid than the NRS ones which have a tenuous and flexible polymeric structure [14,17]. We estimate that such a nice agreement between the simulations and the experiments justifies their presentation in this paper whatever one might think on the crudeness of the experimental procedure.

5.2. THE SCATTERING INTENSITY. — To compare SANS experiments on NRS aerogels with our simulations, we calculated  $I(q)$  for FBA aggregates. This is made possible by multiplying the scattering function  $S(q)$  by a form factor  $P(q)$  characterizing the shape of the particles. Here, we have calculated  $P(q)$  for a cubic particle of size  $l = 2$  divided in  $16 \times 16 \times 16$  sub-cells as the Fourier transform of the sub-particle distance correlation function.

To build FBA gels, simulation were carried out with  $f = 4$  (for reasons given above),  $F = 125$ ,  $c = 0.065$  and  $L = 60$ . The comparison between the numerical curve (solid line) and the experimental data for a NRS aerogel of  $\phi = 0.02$  g/g (circle symbols, shifted vertically and

horizontally for convenience) is presented in Figure 10. It can be seen in this figure that the slopes in the fractal regime are quite similar. Unfortunately, in this model, the relation between the experimental  $\phi$  and the numerical value of  $c$  is not straightforward. Furthermore, for the numerical range of concentrations where a gel can be obtained it is not possible to obtain a fractal domain as extended as that exhibited in the experiments (for which  $\phi_g \ll 0.055$ ). In other words, we are not able to describe quantitatively any crossover, since in our simulations  $\xi$  is only slightly larger than  $a$ , while in experiments it is usual to find up to two decades of fractal domain ( $\xi/a \approx 10^2$ ).

We suspect that the discrepancy between the exponent  $D$  calculated from the mass-distance analysis and the exponent  $D'$  obtained from the slope of  $I(q)$  (and  $S(q)$ ) is due to the pore size distribution, which may be larger in the FBA case than in the DLCA case, as revealed between NRS aerogels and BCS aerogels from thermoporometry experiments [46]. Should the slope of  $I(q)$  be affected by this? Further numerical calculations and experimental tests will be needed in the future to elucidate this point.

## 6. Conclusion

In this work, we have shown that cluster deformations significantly alter the simulated gel structures obtained by a cluster-cluster aggregation mechanism. With cluster deformations a *true* sol-gel transition is obtained at a concentration threshold  $c_g$ . For  $c < c_g$  the saturation of all intra-cluster bounding possibilities prevents the formation of a gelling network while for  $c > c_g$  gelation occurs at a given time  $t_g$  which, in contrast to the DLCA model, does not depend on the box size. The clusters size distribution is also modified and we found evidence that for  $t > t_g$ , a relaxation mechanism induces a slight decrease of the radius of gyration with  $t$ . Moreover, we show that the present model is relevant in several experimental situations. We found that for NRS gels,  $t_g$  does not depend on the container size, in contrast to BCS gels. Hence, gelation under basic catalysis and without addition of catalyst corresponds to small and large flexibility, respectively. Furthermore, there should exist a considerably larger well defined non-zero concentration threshold  $c_g$  in the NRS case than in the BCS case. But such an experimental test will be hard to be made convincingly since BCS gels form a quasi polymeric structure at very low TMOS concentrations [14]. Finally, we have shown that the slope of the fractal regime for our numerical FBA  $I(q)$  curve is in agreement with the slope of the experimental  $I(q)$  curve for NRS aerogels.

## Acknowledgments

We would like to acknowledge discussions with Marie Foret, Jacques Pelous and Thierry Woignier. One of us (A.H.) would like to acknowledge support from CONICIT (Venezuela). The numerical calculations were done on the computers of the CNUSC (Centre National Universitaire Sud de Calcul), Montpellier, France, with support from CNRS.

## References

- [1] Family F. and Landau D.P., Kinetics of Aggregation and Gelation (North-Holland, Amsterdam, 1984).
- [2] Jullien R. and Botet R., Aggregation and Fractal Aggregates (World Scientific, Singapore, 1987).
- [3] Meakin P., Phase Transitions and Critical Phenomena, **12** (Academic Press, New York, 1988) p. 335.

- [4] Meakin P., *Phys. Rev. Lett.* **51** (1983) 1119.
- [5] Kolb M., Botet R. and Jullien R., *Phys. Rev. Lett.* **51** (1983) 1123.
- [6] Hasmy A., Jullien R. and Botet R., *Phys. Rev. Lett.* **75** (1995) 3777.
- [7] González A.E., *Phys. Rev. Lett.* **71** (1993) 2248.
- [8] Sintès T., Toral R. and Chakrabarti A., *Phys. Rev. E* **50** (1994) 3330.
- [9] Hasmy A. and Jullien R., *J. Non-cryst. Solids* **186** (1995) 342.
- [10] Sciortino F. and Tartaglia P., *Phys. Rev. Lett.* **74** (1995) 282.
- [11] González A.E. and Ramírez-Santiago G., *Phys. Rev. Lett.* **74** (1995) 1238.
- [12] Herrmann H.J. and Kolb M., *J. Phys. A* **19** 1986 L1027.
- [13] Hasmy A., Anglaret E., Foret M., Pelous J. and Jullien R., *Phys. Rev. B* **50** (1994) 6006.
- [14] Brinker C.J. and Scherer G.W., *Sol-Gel Science* (Academic Press, New York, 1990).
- [15] Iler R.K., *The Chemistry of Silica* (Wiley, New-York, 1979).
- [16] Keefer K.D., *Better Ceramics Through Chemistry*, C.J. Brinker, D.E. Clark and D.R. Ulrich, Eds., *Mat. Res. Soc. Symp. Proc.* **32** (Pittsburgh, 1984).
- [17] Vacher R., Woignier T., Pelous J. and Courtens E., *Phys. Rev. B* **37** (1988) 6500.
- [18] Hasmy A., Anglaret E. and Jullien R., *Phys. Rev. E* **54** (1996) 4454.
- [19] Carmesin J. and Kremer K., *Macromolecules* **21** (1988) 2819.
- [20] Paul W., Binder K., Heermann D.W. and Kremer K., *J. Chem. Phys.* **95** (1991) 7726.
- [21] Anglaret E., Hasmy A. and Jullien R., *Phys. Rev. Lett.* **75** (1995) 4059.
- [22] Jullien R. and Hasmy A., *Phys. Rev. Lett.* **74** (1995) 4003; *errata* **75**, 2454.
- [23] Turban L. and Debierre J.M., *J. Phys. A* **20** (1987) 4457.
- [24] Stauffer D., *Introduction to Percolation Theory* (Taylor and Francis, London, 1985).
- [25] Binder K., *Rep. Prog. Phys.* **50** (1987) 783.
- [26] Hasmy A. and Jullien R., *Phys. Rev. E* **53** (1996) 1789.
- [27] Gimel J.C., Durand D. and Nicolai T., *Phys. Rev. B* **51** (1995) 11348.
- [28] Lach-hab M., González A.E. and Blaisten-Barojas E. (preprint).
- [29] van Dongen P.G.J. and Ernst M.H., *Phys. Rev. Lett.* **54** (1985) 1396.
- [30] Broide M.L. and Cohen R.J., *Phys. Rev. Lett.* **64** (1990) 2026.
- [31] Meakin P., Vicsek T. and Family F., *Phys. Rev. B* **31** (1985) 564.
- [32] van Garderen H.F., Pantos E., Dokter W.H., Beelen T.P.M. and van Santen R.A., *Mod. Sim. Mater Sci. Eng.* **2** (1994) 295.
- [33] Jullien R. and Kolb M., *J. Phys. A* **17** (1984) L639.
- [34] Brown W. and Ball R.C., *J. Phys. A* **18** (1985) L517.
- [35] Feder J., *Fractals* (Plenum, New York, 1988).
- [36] For illustration see Figure 1 of reference [22].
- [37] Chen S.H. and Teixeira J., *Phys. Rev. Lett.* **57** (1986) 2583.
- [38] Freltoft T., Kjems J.K. and Sinha S., *Phys. Rev. B* **33** (1986) 269.
- [39] Hasmy A., Foret M., Pelous J. and Jullien R., *Phys. Rev. B* **48** (1993) 9345.
- [40] Guinier A. and Fournet J., *Small angle scattering of X-rays* (Wiley Interscience, New-York, 1955).
- [41] Feigin L. and Svergun D., *Structure analysis by small angle X-ray and neutron scattering* (Plenum, New-York and London, 1987).
- [42] Vacher R., Woignier T., Phalippou J., Pelous J. and Courtens E., *J. Non Cryst. Solids* **106** (1988) 161.
- [43] Schaefer D.W., Martin J.E. and Keefer K.D., *Phys. Rev. Lett.* **56** (1986) 2199.
- [44] Porod G., *Kolloid Z.* **124** (1951) 83.
- [45] Schaefer D.W., *MRS Bull.* **XIX** (1994) 49.
- [46] Woignier T., Phalippou J., Quinson J.F., Pauthe M., Reppelin-Lacroix M. and Scherer G.W., *J. Sol-Gel Sci. Technol.* **2** (1994) 277.